Dynamic response of multi-unit floating offshore wind turbines to wave, current and wind loads

Lamei, Azin; Hayatdavoodi, Masoud; Riggs, H. Ronald; Ertekin, R. Cengiz

DOI:
10.1063/5.0172543

Publication date:
2024

Citation for published version (APA):
Lamei, A., Hayatdavoodi, M., Riggs, H. R., & Ertekin, R. C. (2024). Dynamic response of multi-unit floating offshore wind turbines to wave, current and wind loads. *Journal of Renewable and Sustainable Energy*, *16*(2), Article 023307. https://doi.org/10.1063/5.0172543

Dynamic response of multi-unit floating offshore wind turbines to wave, current and wind loads

A. Lamei,[1] M. Hayatdavoodi,[1,2] H.R. Riggs,[3] and R. C. Ertekin[2,4]

[1)] *School of Science and Engineering, University of Dundee, Dundee DD1 4HN, UK*

[2)] *College of Shipbuilding Engineering, Harbin Engineering University, Harbin, China*

[3)] *Civil and Environmental Engineering Department, University of Hawaii, Honolulu, HI 96822, USA*

[4)] *Ocean and Resources Engineering Dep., University of Hawaii, Honolulu, Hawaii 96822, USA*

(*Electronic mail: m.hayatdavoodi@dundee.ac.uk)

(Dated: 14 February 2024)

Motion of a multi-unit wind-tracing floating offshore wind turbine (FOWT) to combined wave-current and wind are obtained in the frequency-domain. The linear diffraction wave theory with a Green function for small current speeds and the blade-element momentum method are used for the hydrodynamic and aerodynamic analysis, respectively. Finite-element method is coupled with the hydrodynamic and aerodynamic equations to obtain the elastic responses of the FOWT to the environmental loads. The wind-tracing FOWT consists of three 5 MW wind turbines installed at the corners of an equilateral triangular platform. The platform is connected to the seabed through a turret-bearing mooring system, allowing the structure to rotate and face the dominant wind direction, hence the multi-unit FOWT is called the wind-tracing FOWT. In this study, rigid-body responses of the wind-tracing FOWT to waves and wind are compared with those to combined wave, current and wind loads for several current speeds and various wave heading angles. For a chosen current speed and wave heading angle, hydro- and aeroelastic responses of the wind-tracing FOWT to combined waves, current and wind are obtained and compared with those of the rigid structure. Discussion is provided on the effect of wave-current interaction on the motion and elastic responses of the wind-tracing FOWT. The numerical results show that under the rated wind speed, the motion of the wind-tracing FOWT is mainly governed by the wave-induced hydrodynamic forces and moments and the presence of current results in larger elastic motion of the FOWT to the environmental loads.

I. INTRODUCTION

Offshore wind turbines with floating substructures experience complex dynamics compared with those on bottom-fixed foundations. The motion of the floating platform is due to the simultaneous effect of waves and current, hydrostatic and mooring restoring forces, and loads due to the aerodynamic load on the rotor and the tower of the wind turbine. As a result of the platform motion of a FOWT, the direction of the incoming flow to the rotor and consequently the aerodynamic load on the wind turbine changes. In addition to the environmental loads, the elasticity of the wind turbine, *i.e.* its blades and tower, and the floating substructure is of great importance for the power output of a FOWT and its motion analysis.

To study the motion of a FOWT due to the environmental loads and its power output, an accurate understanding of the dynamics of the floating substructure and its coupling effect on the wind turbine is essential. High-fidelity methods such as computational fluid dynamics (CFD) provide detailed description of the fluid interaction (water and air) with the FOWTs, see Tran and Kim (2016), Cheng *et al.* (2019) and Zhou *et al.* (2022), among others. However, in practice, CFD calculations, due to the heavy computational demand, can only be applied for a simplified presentation of the wave and wind-interaction with a FOWT such that either the substructure or the entire FOWT is rigid and its motion is constrained to limited degrees of freedom. Hence, high-fidelity methods are not the best option to gain an understanding of the rigid-body and elastic motions of a new concept of FOWTs exposed to the environmental loads. For instance, to the authors' knowledge, high-fidelity methods are not applied to investigate elastic motion of multi-unit FOWTs, where multiple towers are installed on a single platform, subject to simultaneous effect of aerodynamic and hydrodynamic loads.

On the other hand, in design and concept stages of FOWTs, medium- and low-fidelity methods are more desirable as they provide an efficient and fast solution of the dynamic motion of FOWTs due to the environmental loads. Although these methods assume that the motion of the substructure is small, they can include the flexibility of the entire structure of the FOWTs in their motion analysis, see Lamei *et al.* (2023a) and Lamei *et al.* (2023b). In multi-unit FOWTs, due to the large size of the substructure, and the coupling effect between the wind turbines and the substructure, hydro- and aeroelasticity analyses of the entire structure are equally important and should not be neglected. A review of various approaches for the analysis of responses of FOWTs to hydrodynamic and aerodynamic loads can be found in Lamei and Hayatdavoodi (2020).

To date, in high-, medium- and low-fidelity methods, little attention is given to wave-current interaction with single- or multi-unit FOWTs. In addition to the direct effect of current on structures, depending on the current speed, its direction and velocity profile, current interaction with incoming waves can change the wave properties. Hence, the wave-induced hydrodynamic forces on a floating structure might be different when current is present. See Kumar and Hayatdavoodi (2023a,b) for more details on the effect of current on periodic waves in deep and shallow waters, respectively.

The wave-current interaction with a FOWT can be significant considering its mooring system and the geometrical characteristics of the floating platform. For instance, wave-current interaction with a SPAR FOWT results in vortex-induced vibration due to their long cylindrical substructure. Chen *et al.* (2018), Qu *et al.* (2020) and Silva *et al.* (2021) studied the wave-current interaction with a SPAR FOWT using low-fidelity methods and showed that depending on the layout of the mooring system, current effects, in the absence of waves, are confined to static displacement of the mooring lines. However, the wave-current interaction can influence the dynamic motion of the SPAR FOWT significantly.

Several concepts of multi-unit FOWTs with two and three wind turbines have been proposed and their motion to combined wave and wind loads are investigated; see for instance Bae and Kim (2014, 2015), Bashetty and Ozcelik (2020) and Lamei *et al.* (2023a), among others. Multi-unit FOWTs undergo larger hydrodynamic loads due to their large substructures in comparison with single-unit FOWTs. Accordingly, depending on the characteristics of the floating platform and the layout of their mooring system, wave-current interaction may significantly change the hydrodynamic forces and moments on the structure. In a study by Kang *et al.* (2017), the elastic motion of a quadrilateral platform, with four wind turbines, exposed to combined wave, current and wind loads was investigated, and a strong coupling between the elastic motion of the substructure to non-linear waves and the mooring lines was observed. Hence, it is essential to include the wave-current interaction in the hydrodynamic analysis of multi-unit FOWTs. To the authors' knowledge, other than Kang *et al.* (2017), no other study has considered the effect of wave-current-wind interaction with multi-unit FOWTs.

The present study is concerned with comparing rigid-body and elastic motion of the wind-tracing FOWT to combined wave, current and wind loads. The wind-tracing FOWT, introduced by Wong (2015), consists of three 5 MW NREL wind turbines that are supported by a triangular floating platform. The wind-tracing platform is moored with a turret-bearing mooring system that allows the structure to rotate with respect to the turret such that the wind turbines are aligned with the dominant aerodynamic loads on the wind turbines. To identify the preferred location of the turret, Lamei *et al.* (2023b) conducted a parametric study involving the turret location and compared the rigid-body responses of the wind-tracing FOWT to waves aligned and misaligned with wind.

Recently, Lamei *et al.* (2023b,c) developed and introduced a numerical coupling approach for FOWTs in which wave-current-wind interaction with the structure is considered. The numerical approach allows the inclusion of the elasticity of the entire structure, *i.e.* blades, tower and the floating substructure of the FOWTs, and can be applied to both single- and multi-unit FOWTs, see Lamei *et al.* (2023a). The hydro- and aerodynamic analyses are based on low-fidelity methods, the linear diffraction theory for small current speeds and the blade-element momentum method. Furthermore, to include the flexibility of the entire structure, dynamic analysis of the FOWT is coupled with the finite-element method. Using this approach, Lamei *et al.* (2023b) conducted a comparative study on the rigid body responses and elastic motions of single-unit FOWTs, namely a SPAR, a barge and a semisubmersible FOWT to combined wave, current and wind loads. It was shown that motion of the SPAR FOWT undergoes largest changes when current is present in comparison with its motion exposed to waves and wind.

Studying the effect of wave-current-wind interaction on the motion of multi-unit FOWTs is of interest. The wind-tracing FOWT involves unique characteristics in the design of its substructure and mooring layout that are missing in single-unit FOWTs. Therefore, in the present study, the approach by Lamei *et al.* (2023c) is applied to study the dynamic motion of the wind-tracing FOWT to wave, current and wind loads. Due to the presence of multiple wind turbines on the wind-tracing substructure and the large floating platform, hydro- and aeroelastic responses of the multi-unit FOWT might be significant. Thus, it is essential to investigate the elastic deformation of the entire structure of the wind-tracing FOWT and its effect on dynamic motion of the FOWT to various environmental loads. Furthermore, by considering both rigid-body and elastic responses, one can evaluate the importance of elasticity analysis of the FOWT and identify the environmental conditions where its elastic responses are significant.

The theory and the developed numerical approach on hydro- and aeroelastic analysis of FOWTs to the environmental loads are discussed in Section II. Section III presents the rigid-body responses of the wind-tracing FOWT to the environmental loads for various current speeds and misalignments of incoming waves with wind and current. Under the same environmental loading, elastic motion of the wind-tracing FOWT and the structural responses along the towers and the pontoons are presented and discussed in Section V. Finally, concluding remarks on the effect of the wave-current-wind interaction on the elastic motion of the wind-tracing FOWT are provided in Section VI.

II. THEORY AND NUMERICAL SOLUTION

The theory and numerical solution of wave-current-wind interaction with FOWTs is presented and discussed in detail by Lamei *et al.* (2023a,b,c). In this section, the coupling approach is discussed focusing on multi-unit FOWTs.

Shown in Fig. 1, a moving Cartesian coordinate system is defined with its origin on the still-water-level (SWL) and the z-axis positive pointing upwards. The coordinate system is in steady translation with the current speed, U_c along the x-axis. In this study, it is assumed that the incoming wind is orthogonal to the rotor-plane area and codirectional with the x-axis. Furthermore, the incoming current can be in the positive or negative x-directions. Therefore, to model the wave-current misalignment, the wave heading angle, β, changes.

A. Structural analysis

A three-dimensional finite-element model of the blades, the towers and the floating platform is generated with shell elements. Given the material properties of the entire structure, the mass distribution and the structural stiffness matrix are calculated by use of the finite-element method. Furthermore, the mooring lines are modelled with spring elements with a constant stiffness matrix.

The structural deformation of a FOWT is determined by use of a reduced-basis approach, with a subset of m dry modes from the total possible modes of the flexible structure, N. In this approach,

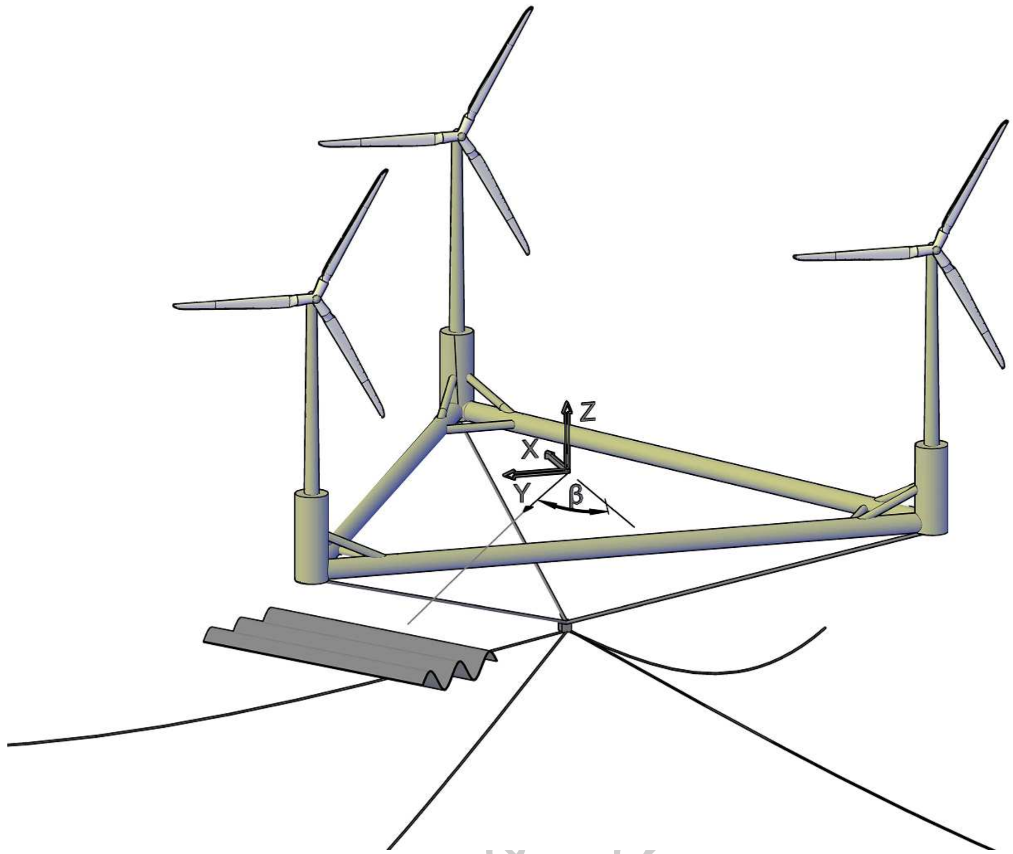

FIG. 1. Schematic of the wind-tracing FOWT, β is the wave heading angle, given with respect to the *x*-axis.

m modes are chosen such that they are sufficient to represent the flexibility of the blades, the tower and the floating platform. Hence, the flexibility of the FOWTs is defined by a linear superposition of *m* modes and are included in the total degrees of freedom of the FOWTs in their equation of motion.

The hydrostatic restoring coefficients of flexible FOWTs are computed by an explicit formulation that accounts for the change in hydrostatic pressure and the internal stresses of the structure, see Huang and Riggs (2000) for more details.

B. Wave-current interaction with a floating structure

Wave-current interaction with a FOWT is studied within the context of the linear diffraction theory for small current speeds, $\tau = \frac{U_c\,\omega_e}{g} \leq 0.25$, where U_c is the current speed, ω_e is the encounter wave frequency, and g is the gravitational acceleration. In this approach, the fluid is inviscid and incompressible and the flow is irrotational. Waves are assumed of small-amplitude and the motions and rotations of the structure due to waves and current are linearly proportional to the wave amplitude. In this method, the current direction is parallel to the x-axis, and waves can propagate with an arbitrary angle, β, with respect to the x-axis, see Fig. 1. ω is the incoming wave frequency and the encounter frequency in the moving coordinate system is given as

$$\omega_e = \omega - |U_c|\,k\,\cos(\beta), \tag{1}$$

where k is the incoming wave number.

Assuming that the current speed is small, the total velocity potential can be given as the sum of the steady velocity potential $\bar{\phi}_s$ due the local steady flow by current, and a harmonic velocity potential:

$$\Phi\,(x,y,z,t) = |U_c|\,(\bar{\phi}_s - x) + \Re\{\phi\,e^{i\,\omega_e\,t}\}. \tag{2}$$

in which ϕ is the sum of incident wave velocity potential, ϕ^I, the linear velocity potential due to the wave diffraction-radiation, ϕ^L, and the linear term representing the interaction of the steady flow with the wave diffraction-radiation, ϕ^N, *i.e.*

$$\phi\ =\ \phi^I + \phi^L + \phi^N. \tag{3}$$

The incoming waves velocity potential is known analytically and ϕ^L and ϕ^N are obtained given the boundary conditions on the wetted surface of the body and the free surface at the vicinity of the floating structure. ϕ^L and ϕ^N satisfy homogeneous and non-homogeneous boundary conditions on the free surface, respectively:

$$-\frac{\omega_e^2}{g}\phi^L + 2i\tau\frac{\partial\phi^L}{\partial x} + \frac{\partial\phi^L}{\partial z} = 0, \quad \text{on } S_F, \tag{4}$$

$$-\frac{\omega_e^2}{g}\phi^N + 2i\tau\frac{\partial\phi^N}{\partial x} + \frac{\partial\phi^N}{\partial z} = Q, \quad \text{on } S_F, \tag{5}$$

where Q is defined by

$$Q = 2\,i\nabla\bar{\phi}_s\,\nabla(\phi^I + \phi^L) - i\,(\phi^I + \phi^L)\,\frac{\partial^2\bar{\phi}_s}{\partial z^2}, \quad \text{on } S_F. \tag{6}$$

Furthermore, the boundary conditions of ϕ^L and ϕ^N on the body surface are given in diffraction and radiation problems. The boundary conditions in diffraction problems are:

$$\frac{\partial\phi^L}{\partial n} = -\frac{\partial\phi^I}{\partial n}, \qquad \frac{\partial\phi^N}{\partial n} = 0, \quad \text{on } S_B. \tag{7}$$

In the radiation problem, the boundary conditions are satisfied in translational and rotational degrees of freedom of the floating structure, and, if the hydroelastic motion of the body to waves and current is of interest, the computed generalised modes of the structure. The boundary conditions of ϕ^L and ϕ^N on the body surface for the radiation problem are:

$$\frac{\partial\phi^L}{\partial n} = n_j, \qquad \frac{\partial\phi^N}{\partial n} = \frac{i\,m_j}{k}, \quad j = 1, 2, \cdots, m, \text{ on } S_B, \tag{8}$$

where m_j terms represent the change in the current-induced local steady flow due to the motion and deformation of the body. Formulations of the m_j terms for rigid-body and the generalised modes are presented in Wu (1984), Wu and Taylor (1990), Wu (1991) and Chen and Malenica (1998). Finally, the steady velocity potential, $\bar{\phi}_s$ is obtained by its boundary conditions on the body and free surface:

$$\frac{\partial \bar{\phi}_s}{\partial z} = 0, \quad \text{on } S_F, \tag{9}$$

$$\frac{\partial \bar{\phi}_s}{\partial n} = n_1, \quad \text{on } S_B, \tag{10}$$

where n is the normal vector on the body surface, $n = (n_1, n_2, n_3)$, pointing out of the fluid. Given the boundary conditions on the wetted surface of the body and the free surface, the steady velocity potential, $\bar{\phi}_s$ and harmonic velocity potentials, ϕ^L and ϕ^N, are determined by boundary-integral method using the Green function for small current speeds. The Green function for wave-current interaction with a floating structure with small current speeds have been developed generally in two approaches, *(i)* perturbation method, *i.e.* expansion of the Green function with respect to τ (see *e.g.* Nossen *et al.* (1991), Ertekin *et al.* (1994), Padmanabhan and Ertekin (2003) and Padmanabhan and Ertekin (2011)) or *(ii)* a Green function given as a sum of a term due to the wave diffraction-radiation problem and terms due to the presence of the local steady flow by the current, (see Noblesse *et al.* (1995), Chen and Malenica (1998) and Monroy *et al.* (2012)). In this study, the latter approach for the Green function is implemented, see Noblesse *et al.* (1995) and Chen and Malenica (1998) for the formulation of the Green function and the boundary-integral equations.

Finally, first-order hydrodynamic excitation forces and moments are:

$$\begin{aligned} F_j^{exc} = -i\,\rho_w \omega_e \iint_{S_B} (\phi_j^I + \phi_j^L + \tau\phi_j^N)\, n_j\, dS + \\ \frac{\rho_w\, g}{\omega_e} \iint_{S_B} \nabla\,(\bar{\phi}_s - x)\,\nabla(\phi_j^I + \phi_j^L) n_j\, dS. \end{aligned} \tag{11}$$

The added-mass, a_{jk}, and hydrodynamic damping, b_{jk}, coefficients are obtained from R_{jk}

$$R_{jk} = -i\,\rho_w \omega_e^2 \iint_{S_B} (\phi_{jk}^L + \tau\phi_{jk}^N)\, n_k\, dS - \\ i\,\rho_w\, g \iint_{S_B} \nabla\,(\bar{\phi}_s - x)\,\nabla(\phi_{jk}^L)\, n_k\, dS, \tag{12}$$

where

$$a_{jk} = \Re\Big\{\frac{1}{\omega_e^2} R_{jk}\Big\}, \qquad b_{jk} = \Im\Big\{\frac{1}{\omega_e} R_{jk}\Big\}. \tag{13}$$

Given the excitation forces and moments on the floating structure (sum of the Froude-Krylov and diffraction forces and moments) and those due to the added-mass and hydrodynamic damping coefficients, the equations of motion of the floating structure to combined waves and current are

$$\xi_j[-\omega_e^2(M_{ij}+a_{ij})+i\omega_e(b_{ij})+(c_{ij,moor}+c_{ij})] = AF_i^{exc}\,, \quad i,j=1,2,\cdots m, \tag{14}$$

where c_{ij} and $c_{ij,moor}$ are the hydrostatic restoring and the mooring line stiffness coefficients, respectively. The response amplitude operators (RAOs), $|\frac{\xi_j}{A}|$ of the floating structure to waves and current are computed for a range of encounter frequencies, ω_e.

C. Aerodynamic loads on wind turbines

Assuming that the wind speed is constant and the incoming wind flow is orthogonal to the rotor-plane area, the aerodynamic loads on the rotors of a FOWT are computed by use of the steady blade-element momentum method (BEM). The theory is described in detail by Hansen *et al.* (2006), among others, and its application in our numerical approach is discussed for single and multi-unit FOWTs in Lamei *et al.* (2023a,b,c). In this approach, to include the wind-wave misalignment, the wave heading angle, β, changes. Furthermore, the wake-interaction between the rotors supported by the same structure is not considered.

To obtain the motion of a FOWT to the environmental loads in the frequency-domain, the aerodynamic loads on the rotor and the tower are linearised with a harmonic function with encounter wave frequency, ω_e. Assuming that the thrust force on the rotors is an excitation force that is transferred to the tower tops and given that the towers commonly have circular cross-sections, the phase angle of the aerodynamic excitation force, $F_{j,W}$ is computed by the same formulation given by MacCamy and Fuchs (1954) for harmonic excitation forces on circular cylinders. Thus, the complex wind excitation force on the rotor is given as

$$F_{j,W} = |F_{j,W}| \cos(\omega_e t - \delta_{\text{aero}}), \quad j = 1, 2, \cdots, m, \tag{15}$$

where δ_{aero} is the phase angle of the excitation force and it is given by

$$\delta_{\text{aero}}(k_e r_0) = -\tan^{-1}\left[\frac{Y_1'(k_e r_0)}{J_1'(k_e r_0)}\right], \tag{16}$$

where k_e is the encounter wave number, $J_p(k_e r)$ and $Y_p(k_e r)$ are the Bessel functions of the first and the second kind of order p, respectively, and r_0 is the top diameter of the tower.

Due to the motion of the substructures of FOWTs, rotors experience a relative motion with respect to the incoming wind flow. Therefore, in steady BEM, the thrust force on a rotor of a FOWT is given as a function of the relative incoming wind speed on the rotor, $V_{rel} = V_0 - V_h$, where V_0 is the incoming wind speed and V_h is the horizontal speed of the rotor hub, along the incoming wind direction. Therefore, the thrust on the rotor of a FOWT is:

$$T(V_{rel}) = \frac{1}{2}\rho_a A_r C_T (V_{rel}^2), \tag{17}$$

where ρ_a is the air density, A_r is the rotor-plane area, and C_T is the thrust coefficient. In the frequency-domain, the hub velocity in the x-direction can be given as $i\omega_e(\xi_1+\xi_5(z_h-z_{cg}))$ for the rigid structure, where z_h and z_{cg} are the vertical coordinates at the hub and the centre of gravity, respectively. Assuming that V_h is small and the thrust force due to $O(V_{rel}^2)$ and higher terms are negligible, Eq. (17) is simplified as

$$T(V_{rel}) = \frac{1}{2}\rho_a A_r C_T (V_0^2) - \rho_a A_r C_T (V_0\, i\omega_e(\xi_1+\xi_5(z_h-z_{cg}))). \tag{18}$$

in which the first term in Eq. (18) represents the excitation aerodynamic force in surge, $F_{1,W}$, on a fixed rotor, *i.e.* $V_h=0$. Furthermore, the second term on the right-hand side of Eq. (18) is due to the relative motion of the hub along the incoming wind direction, where $\rho_a C_T V_0$ represents the aerodynamic damping coefficient, $B_{aero,11}$, on a FOWT with a single rotor. For an arbitrary FOWT with n wind turbines, the aerodynamic damping matrix in the translational and rotational modes is

$$B_{aero} = \begin{bmatrix} n\times(\rho_a C_T A_r V_0) & 0 & 0 & 0 & -\sum_{j=1}^{n}\rho_a C_T A_r V_0(z_h^j - z_{cg}) & -\sum_{j=1}^{n}\rho_a C_T A_r V_0(y_h^j - y_{cg}) \\ 0 & 0 & 0 & 0 & 0 & 0 \\ 0 & 0 & 0 & 0 & 0 & 0 \\ 0 & 0 & 0 & 0 & 0 & 0 \\ -\sum_{j=1}^{n}\rho_a C_T A_r V_0(z_h^j - z_{cg}) & 0 & 0 & 0 & \sum_{j=1}^{n}\rho_a C_T A_r V_0(z_h^j - z_{cg})^2 & 0 \\ -\sum_{j=1}^{n}\rho_a C_T A_r V_0(y_h^j - y_{cg}) & 0 & 0 & 0 & 0 & \sum_{j=1}^{n}\rho_a C_T A_r V_0(y_h^j - y_{cg})^2 \end{bmatrix}, \tag{19}$$

and the aerodynamic load vector is

$$F_W = \begin{bmatrix} \sum_{j=1}^{n} |F_{1,W}^j| \cos(\omega_e t - \delta_{\text{aero}}^j) \\ 0 \\ 0 \\ 0 \\ -\sum_{j=1}^{n} |F_{1,W}^j| \times (z_h^j - z_{cg}) \cos(\omega_e t - \delta_{\text{aero}}^j) \\ -\sum_{j=1}^{n} |F_{1,W}^j| \times (y_h^j - y_{cg}) \cos(\omega_e t - \delta_{\text{aero}}^j) \end{bmatrix}, \tag{20}$$

Furthermore, the drag force by the incoming wind on the towers are computed with an empirical relation

$$F_D = \frac{1}{2} C_d A_t V_0^2 \tag{21}$$

where $C_d = C_d(Re)$ is the drag coefficient with respect to the incoming wind Reynolds number, $Re = \frac{V_0 D}{\nu}$, with D the diameter of the tower, ν is the air kinematic viscosity at 20°, and A_t is the cross-sectional area of the tower. Similar to the wind excitation forces on the rotors, the phase angle of the aerodynamic drag force on the towers is computed by Eq. (16).

If the elasticity of the FOWT is of interest, the aerodynamic forces and damping coefficients in the generalised modes are obtained by use of the finite-element method. Finally, given the total aerodynamic damping matrix and the excitation load vector at the centre of gravity of the FOWT, Eqs. (19) and (20), respectively, the motion of the structure to combined wave, current and wind is determined in the frequency domain. Therefore, F_W and B_{aero} are added to the right-hand and the left-hand sides of the equations of motion of a floating structure, Eq. (14), respectively:

$$\xi_j[-\omega_e^2(M_{ij}+a_{ij}) + i\omega_e(b_{ij} + B_{aero,mat}) + (c_{ij,moor} + c_{ij})] = AF_i^{exc} + F_{i,W} \qquad i,j = 1,2,\cdots m, \tag{22}$$

where the rigid-body responses, for $m = 6$, and the elastic motion, for $m > 6$, of the FOWTs to waves, current and wind are obtained by solving Eq. (22) for the encounter wave frequency, ω_e.

D. Numerical solution

The numerical solution of wave-, current- and wind-interaction with a FOWT is implemented in HYDRAN-XR, see NumSoft Technologies (2023). HYDRAN-XR is a potential-flow solver for wave-induced hydrodynamic analysis that is integrated with the finite-element method to include the elastic motion of the floating body. Lamei *et al.* (2023a) and Lamei *et al.* (2023c) further enhanced HYDRAN-XR to include a Green function for combined waves and small current speeds to account for wave-current-structure interaction, and BEM to determine aerodynamic loads on FOWTs.

Given the finite-element model of the FOWTs, the mass and stiffness matrices of the structure are calculated. Furthermore, the aerodynamic thrust force and aerodynamic damping effect on the rotor are applied as nodal forces and dampers to the nodes on the blades, facing the incoming wind. The pressure difference upstream and downstream the towers results in an aerodynamic drag force. In the developed numerical model, the drag forces on the towers are modelled as distributed nodal forces on their front faces, *i.e.* those areas of the towers that face the incoming wind. The equivalent aerodynamic excitation load vector and damping matrix at the centre of gravity of the structure are determined by use of the finite-element method. Next, the finite-element model of the FOWT is conformed to a panel mesh with a one-to-one mapping over the wet surface of the platform. Furthermore, panel mesh on the free surface at the vicinity of the floating structure is generated. Next, wave-current-structure interaction is solved by use of a three-dimensional source distribution, the Green function method. Finally, the equation of motion of the FOWT to combined waves, current and wind, Eq. (22), is solved to determine the rigid-body responses and, if elasticity is considered, the elastic motion of the structure, at a given encounter wave frequency, ω_e.

III. THE WIND-TRACING FOWT

The wind-tracing FOWT is a multi-unit FOWT that consists of three 5 MW NREL wind turbines supported by the columns of the floating platform, see Lamei *et al.* (2023b). The columns are connected to three pontoons with a length of $2.2\,D_r$, where D_r is the rotor diameter. The length of the pontoons are specified such that the aerodynamic wakes of the front rotors potentially have minimal interference with the performance of the rear rotor. The unique characteristic of the wind-tracing FOWT is in its mooring mechanism, the turret-bearing mooring system.

Lamei *et al.* (2023b) conducted a parametric study on the layout of the turret-bearing mooring system of the wind-tracing FOWT and identified the preferred location of the turret. The turret is submerged $4\,d$ under the platform, where $d = 16$ m is the draft of the wind-tracing FOWT, see Fig. 2(b). Furthermore, in the *xy*-plane, the turret is located $1/6$ L away from Column 1, where L is the horizontal distance between Column 1 and Pontoon 3, see Fig. 2(a). The turret is connected to the bottom of the columns and the seabed with three taut cables and four catenary mooring lines, respectively. Here, the turret is modelled as $2 \times 2 \times 2$ m rigid box, and the taut cables are connected to a universal joint at the top of the turret. Furthermore, the catenary mooring lines are attached to the four corners at the bottom of the turret. This layout of the mooring lines allows the platform to rotate about the z-axis freely with respect to the turret, and it is constrained in its roll and pitch modes as it is connected to the catenary mooring lines at its four bottom corners.

The geometry and the material properties of the wind-tracing platform, the mass distribution and the hydrostatic properties of the FOWT considered here, are presented in detail by Lamei *et al.* (2023b), who also performed a mooring analysis of the wind-tracing FOWT. These properties are summarised in Table I. Furthermore, Table II presents the computed wet natural periods of the

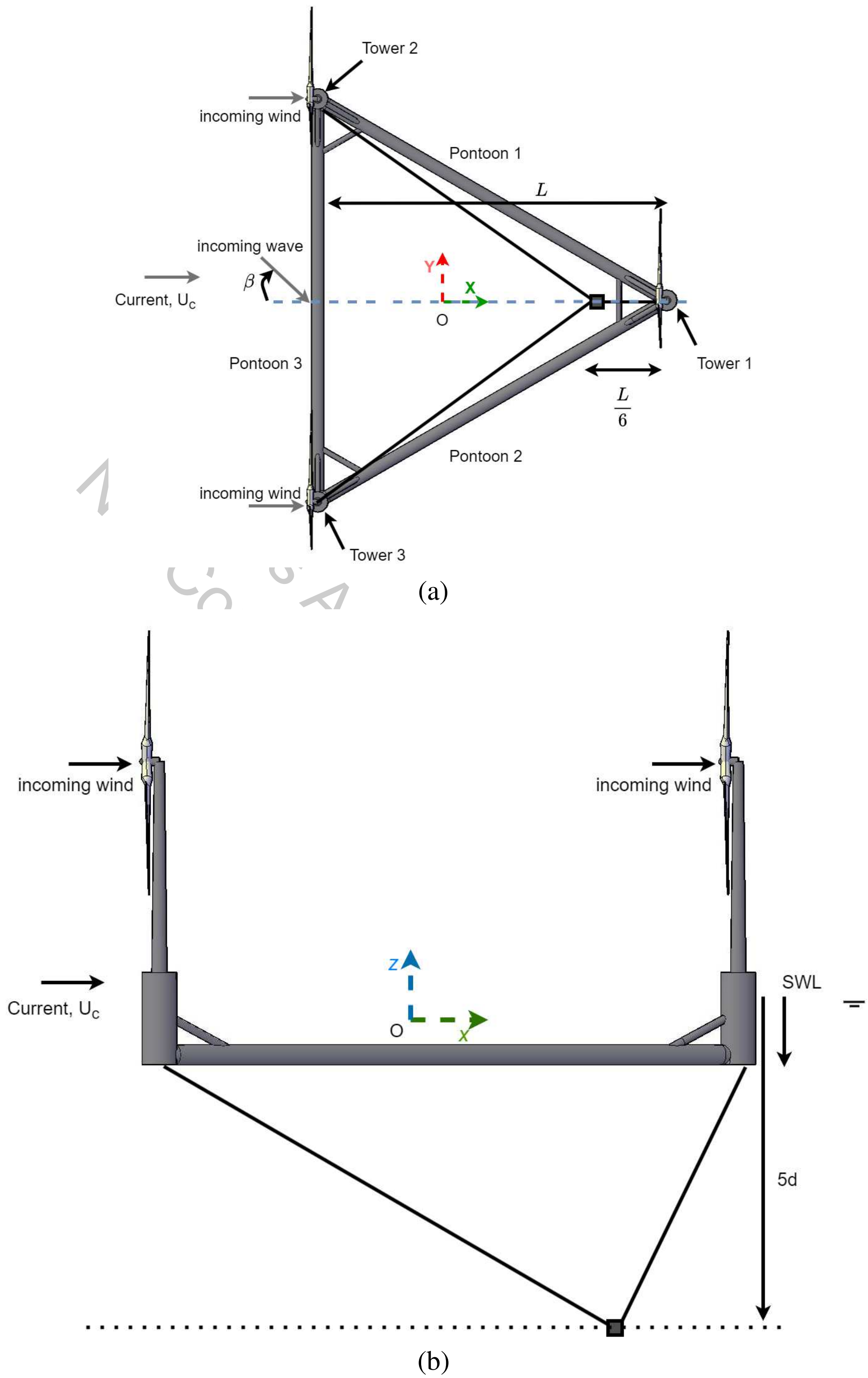

FIG. 2. (a) Top- and (b) side-view of the wind-tracing FOWT and its turret-bearing mooring system. The solid lines and the box represent the taut cables and the turret, respectively.

rigid and flexible FOWT in heave, roll and pitch modes.

TABLE I. The mass distribution of the wind-tracing FOWT and the properties of its mooring layout.

Mass distribution and hydrostatic properties	
Mass of the structure (without ballast)	23099 tonnes
Total mass of the turret	64.3 tonnes
Ballast mass	23718 tonnes
Displaced volume	4.7001×10^4 m^3
Centre of gravity (CG)	7.60 m below SWL
Centre of buoyancy (CB)	11.2 m below SWL
Roll inertia about CG	3.55×10^{11} kg-m^2
Pitch inertia about CG	3.58×10^{11} kg-m^2
Yaw inertia about CG	6.85×10^{11} kg-m^2
Mooring lines properties	
Centre of geometry of the turret	(20.03 m, 0 m, −80 m)
Taut diameter	153 mm
Taut axial stiffness	1481 MN/m
Catenary diameter	95 mm
Catenary wet weight	1942.4 N/m

Here, the wave-current-wind interaction with the wind-tracing FOWT under various environmental loadings are investigated. Firstly, assuming that the entire structure of the wind-tracing FOWT is rigid, its motion due to the wave-current-wind combination is obtained and discussed. Next, the elastic responses of the structure are obtained and compared with its rigid-body counter-

TABLE II. Wet natural periods of the rigid and flexible wind-tracing FOWT in heave, roll and pitch modes.

Mode	Rigid structure	Flexible structure
Heave	27.78 s	26.8 s
Roll	21.42 s	21.1 s
Pitch	20.44 s	21.1 s

parts. Shown in Fig. 2(a) and (b), the origin of the body-fixed coordinate system is at the centre of gravity along a vertical line passing through the centre of geometry of the triangular platform and 7.60 m under the SWL. In the following sections, the incoming waves have unit amplitude and the wind speed is fixed at $V_0 = 11.4$ m/s, the rated wind speed of the 5 MW NREL wind turbines. Following the linear wave theory assumptions for wave-current interaction, the current speeds are chosen such that $\tau < \frac{1}{4}$, see Section II. In this study, unless otherwise stated, the current speed is constant at $U_c = 0.8$ m/s and always parallel to the *x*-axis. The current is assumed uniform across the water depth, and may be codirectional or in opposite direction of the *x*-axis. Finally, in the following sections, the results are presented as a function of the encounter wave period. The simulations are carried out on a desktop machine with Intel Core *i*5 6500U, 3.20 GHz CPU and 32 GB memory and took approximately 6 days for 35 wave periods.

IV. RIGID-BODY RESPONSES

Prior to obtaining the responses of the wind-tracing FOWT, the wave-induced excitation forces and moments on the structure are determined and compared with those when current is also present. In this section, the current is always perpendicular to the structure, *i.e.* parallel to the *x*-axis with $U_c = 0.8$ m/s and the waves are either in the following ($\beta = 0°$) or opposing ($\beta = 180°$) directions. The horizontal and vertical excitation forces, F_x^{exc} and F_y^{exc}, and the excitation moment

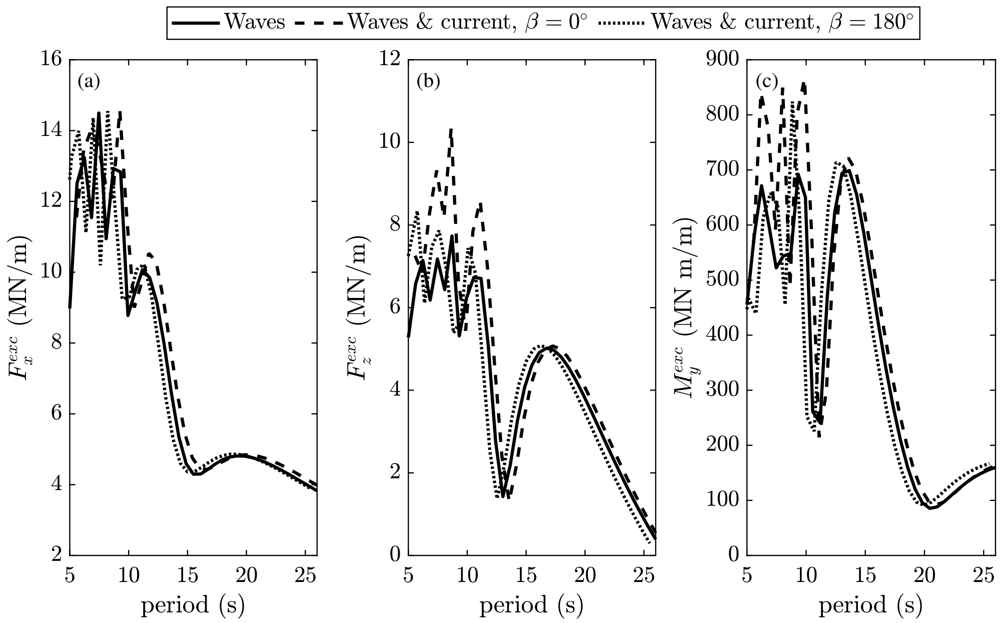

FIG. 3. Comparison of excitation forces in (a) surge F_x^{exc}, (b) heave F_z^{exc}, and (c) excitation moment in pitch, M_y^{exc}, on the wind-tracing FOWT due to waves with those due to combined waves and current, with $\beta = 0°$ and 180° and $U_c = 0.8$ m/s.

in pitch, M_y^{exc} are presented in Fig. 3. When current is present and codirectional with the incoming waves, the excitation forces in surge and heave and the excitation moment in pitch increase slightly. Furthermore, shown in Fig. 3, current interaction with opposing waves results in smaller excitation forces and moment on the floating structure compared with those due to waves and those due to current interaction with following waves. However, in general, the presence of current does not influence significantly the excitation forces and moments on the wind-tracing FOWT.

Next, the rigid-body responses of the wind-tracing FOWT in three environmental conditions, namely *(i)* waves only, *(ii)* combined waves and current (in the absence of wind) and *(iii)* combined waves and wind (in the absence of current) are presented in Fig. 4. It should be noted that the airfoil profile varies along the blade, resulting in an asymmetric blade. Hence, although the wind-tracing platform is symmetric, the complete structure, *i.e.* the platform and the wind turbines, is not symmetric and as a result its motion in roll is coupled with its motions in its heave and pitch modes. Commonly, surge, heave and pitch RAOs undergo a peak at approximately 22 s, which is close to the roll and pitch natural frequencies of the rigid wind-tracing FOWT, see Table II. Moreover, at $T_e = 27$ s, approximately the wet natural period of the rigid structure in heave (see Table II), a peak is observed in waves- and wind-induced heave RAOs, and there is a trough in heave RAOs to waves and combined waves and current. The peak observed in surge and heave RAOs of the structure are due to their couplings with its pitch and roll motions. Furthermore, it is observed that the addition of the aerodynamic loads results in slightly smaller surge RAOs and larger pitch RAOs compared with the wave-induced and combined wave- and current-induced surge and pitch motions for encounter wave periods 10 s $\leq T_e \leq$ 20 s. The total aerodynamic thrust force and the moment in pitch mode on the wind-tracing FOWT are 2.45 MN and 284.9 MNm, respectively, which are significantly smaller than the wave-induced hydrodynamic forces and moment, see Fig. 3. Hence, the small changes in surge and pitch RAOs of the structure when aerodynamic loads are present can be explained by the effect of the aerodynamic damping due to the operating rotors of the FOWT combined with the hydrodynamic damping coefficient. For the same interval of encounter wave periods, wave-current interaction results in smaller heave motion compared with those to waves only and combined waves and wind.

Shown in Figs. 3 and 4, the effect of current on excitation forces and moments, and the rigid-body motion of the wind-tracing FOWT is relatively small. Similarly, considering the motion of the wind-tracing FOWT to combined waves and wind, it is observed that wave-induced hydrodynamic forces and moments are the dominating terms in dynamic motion of the structure.

A. Effect of current speed

As discussed earlier in this section, wave-current interaction with the wind-tracing FOWT and current speed of 0.8 m/s, resulted in small changes in its dynamic motion compared with its wave-induced rigid-body responses. In this section, we investigate the effect of current speed and its

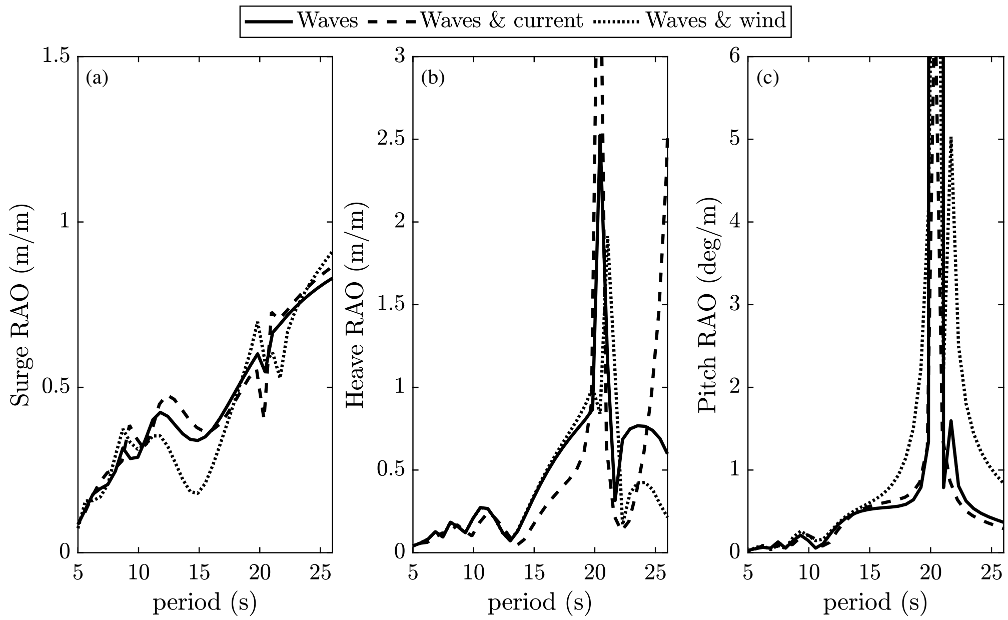

FIG. 4. Comparison of the rigid-body responses of the wind-tracing FOWT to *(i)* waves only, *(ii)* combined waves and current with current speed at $U_c = 0.8$ m/s and *(iii)* combined waves and wind, with wind speed of $V_0 = 11.4$ m/s.

direction with respect to the x-axis on the dynamic motion of the wind-tracing FOWT.

The wave-current-wind interaction with the wind-tracing FOWT is studied for various current speeds and discussed. For this purpose, six current speeds, ± 0.6 m/s, ± 0.8 m/s and ± 1.2 m/s are considered. The incoming waves are at zero wave heading angle, and positive and negative current speeds indicate that the current is in following or opposing direction of headsea waves, respectively. Shown in Fig. 5, surge, heave and pitch motions of the rigid wind-tracing FOWT to combined wave, current and wind are determined for the given current speeds and compared with those in the absence of current.

It is observed that for currents in the following direction of incoming waves, as the current speed becomes larger, the surge motion of the structure increases slightly for encounter wave periods smaller than approximately $T_e = 16$ s. Regarding the encounter wave periods smaller than $T_e \leq 20$ s, the heave motion of the wind-tracing FOWT is larger with current in opposing direction of incoming waves. Moreover, the largest effect of current speed is observed in heave

RAOs of the rigid wind-tracing FOWT, particularly at wave periods larger than $T_e = 22$ s. The significant increase in heave motion of the FOWT is observed in an interval of encounter wave periods between the pitch and heave natural periods of the structure, see Table II. Finally, for $T_e \leq 18$ s and $T_e \geq 22$ s, the effect of the current speed on the pitch motion of the wind-tracing FOWT is almost negligible, while it becomes more significant at approximately 18 s $\leq T_e \leq$ 22 s, around the wet natural period in pitch mode.

In general, by changing the current speed and its direction with respect to the incoming waves, the surge and heave motion of the wind-tracing FOWT undergo significant changes at encounter wave periods closer to the wet natural periods of the structure in pitch, roll and heave. However, the effect of current speed on the pitch motion of the FOWT is almost negligible.

B. Effect of wave direction

In this section, the effect of wave misalignment with current and wind loads on the motion of the wind-tracing FOWT is investigated. RAOs of the structure to combined waves, current and wind are presented in Fig. 6 for wave heading angles $\beta = 0°$, $30°$, $45°$, $90°$ and $180°$. The current and the wind speeds are constant at $U_c = 0.8$ m/s and $V_0 = 11.4$ m/s, respectively. In all cases, the current is codirectional with the x-axis and perpendicular to the structure.

Shown in Fig. 3, the motion of the structure is primarily governed by wave-induced forces and moments. In Fig. 6(c), relatively similar pitch RAOs of the FOWT are observed to codirectional and misaligned waves, current and wind for encounter wave periods up to approximately 20 s. At 20 s, approximately the pitch wet natural period of the structure, the peak value of the pitch RAO to codirectional wave, current and wind is the largest compared with those for $\beta > 0°$. At the same encounter wave period, shown in Fig. 3, the horizontal excitation force and moment in pitch by codirectional waves and current are larger than those to waves and current in opposite direction. It

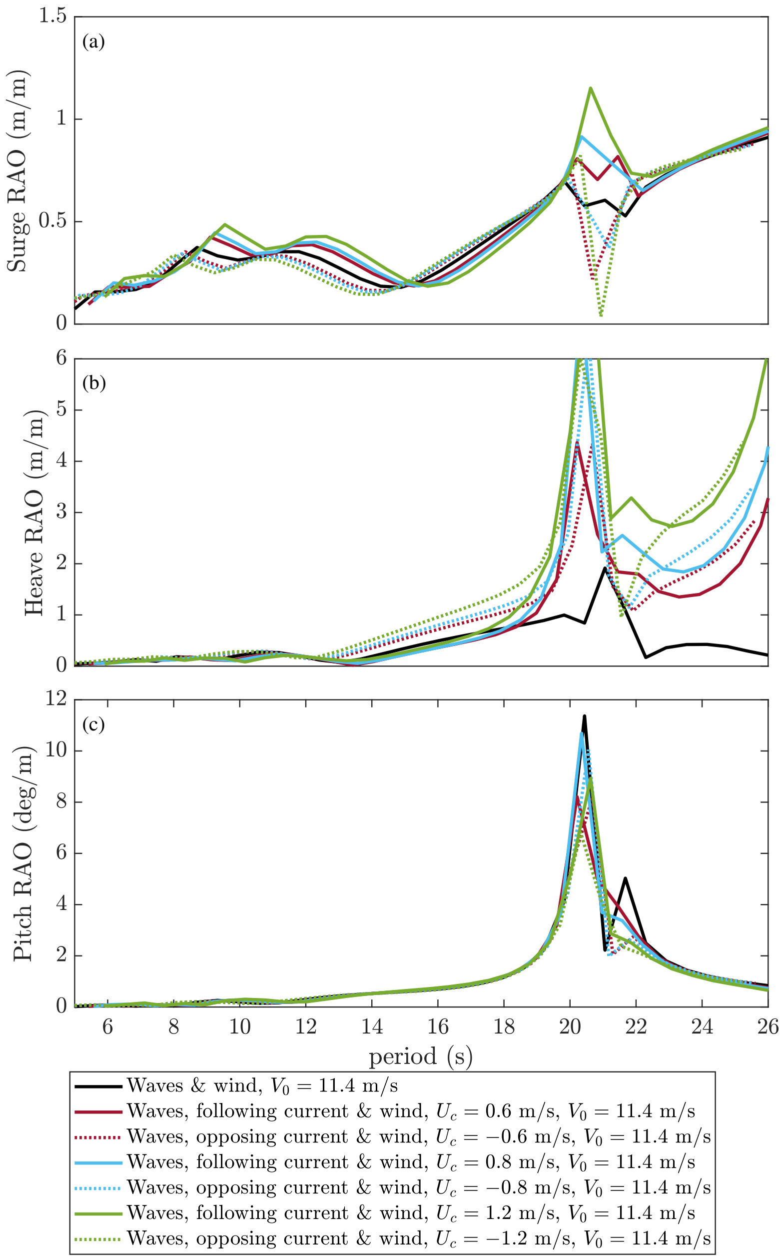

FIG. 5. Surge, heave and pitch motions of the rigid wind-tracing FOWT to waves and wind in the absence of current, and waves, current and wind with current speeds $U_c = \pm 0.6$ m/s, $U_c = \pm 0.8$ m/s and $U_c = \pm 1.2$ m/s and $V_0 = 11.4$ m/s.

is observed that the misalignment of incoming waves with current and wind has the largest effect on the surge motion of the floating structure. It can be seen that up to the encounter wave period of 16 s, the surge motion of the structure to codirectional waves, current and wind is the largest compared with other load cases. Furthermore, for wave periods approximately larger than 14 s, the heave and pitch RAOs of the structure are the smallest to beam waves ($\beta = 90°$) combined with the horizontal current and wind loads on the wind-tracing FOWT. The peak in surge RAOs is shifted to a larger wave period with wave heading angle $\beta = 180°$. Moreover, with waves in opposing direction of current and wind, the large peaks observed in heave and pitch RAOs are shifted to larger encounter wave periods and are approximately at the wet natural period in the roll mode.

Shown in Fig. 6, the misalignment of incoming waves with the current and wind can significantly change the surge RAOs of the wind-tracing FOWT. The effect of wave heading angle on the heave and pitch motion of the structure is significant in long wave periods larger than approximately 18 s $\leq T_e$.

V. FLEXIBLE-BODY RESPONSES

In this section, the hydro- and aeroelastic motion of the wind-tracing FOWT to the environmental loads are presented and discussed. Firstly, wave-current-wind interaction with the fully flexible wind-tracing FOWT is studied by presenting its motions in surge, heave and pitch modes. Next, nodal displacements along the towers and pontoons of the flexible FOWT are determined and compared with its rigid-body counterparts.

Shown in Fig. 7, rigid- and flexible-body responses of the wind-tracing FOWT to wave, current and wind loads are obtained and compared. Firstly, it can be seen that for 14 s $\leq T_e$, the rigid structure undergoes smaller surge motions than those of the flexible structure. Similarly, the heave motion of the rigid FOWT is smaller than the flexible wind-tracing FOWT for encounter wave periods $T_e \leq 20$, which is close to the roll and pitch natural periods of the flexible structure, see Table II. Finally, for the majority of the considered encounter wave periods, the rigid-body pitch RAOs to the combined waves, current and wind are larger than those of the flexible structure. The

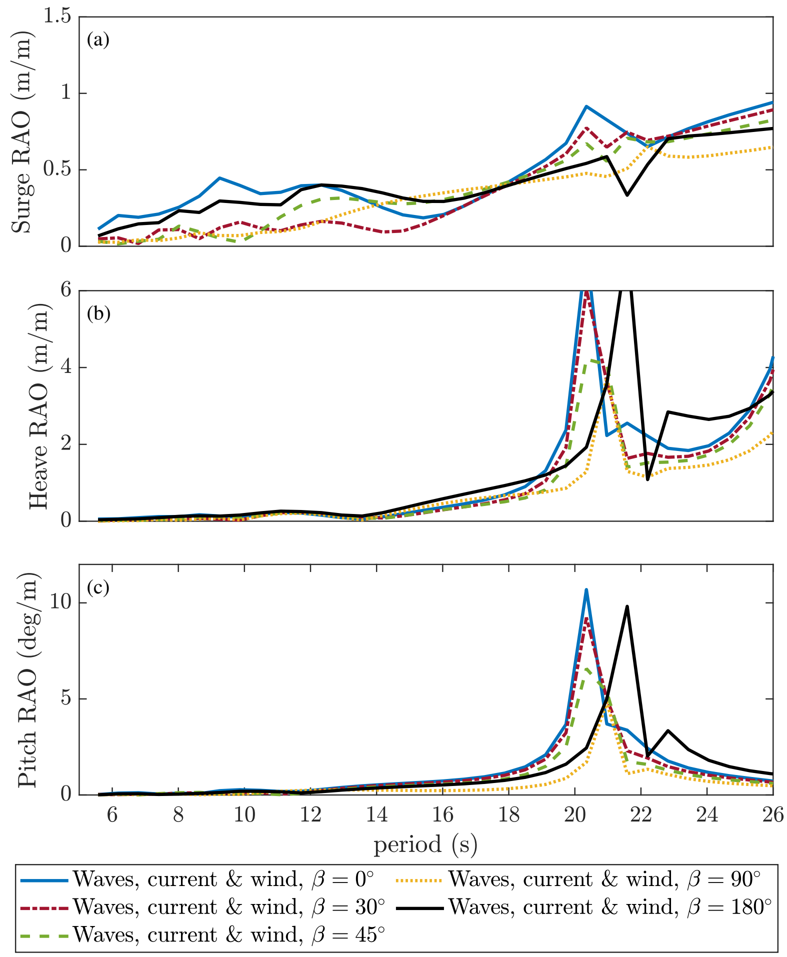

FIG. 6. (a) Surge, (b) heave and (c) pitch motions of the rigid wind-tracing FOWT to codirectional waves, current and wind, and waves misaligned with current and wind with $\beta = 30°, 45°, 90°$ and $180°$, $V_0 = 11.4$ m/s and $U_c = 0.8$ m/s.

peak of the pitch RAOs of the flexible structure is smaller than the one of the rigid wind-tracing FOWT, and as expected, occurs at approximately 21 s.

Next, the effect of flexibility of the wind-tracing FOWT on its structural responses to hydro- and aerodynamic loads is investigated. For this purpose, nodes at the leading edge of the towers, starting from their bases, $z = 22$ m, up to the tips of the towers, $z = 109$ m, facing the incoming wind, and nodes on the outer edge of the pontoons, facing outside the triangular platform at $z = -12$ m are considered. The horizontal nodal displacements along the towers are due to the motion of the structure in its surge and pitch modes, and if elasticity considered, its generalised modes.

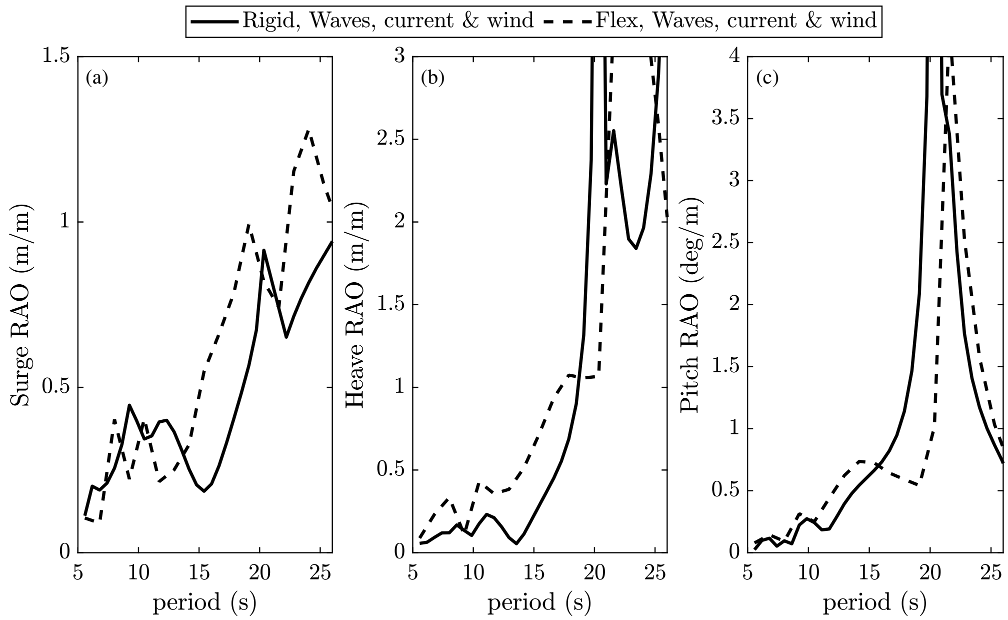

FIG. 7. (a) Surge, (b) heave and (c) pitch motions of the rigid and flexible wind-tracing FOWT to codirectional waves, current and wind, with $V_0 = 11.4$ m/s and $U_c = 0.8$ m/s.

Furthermore, the vertical nodal displacements along the pontoons are a result of the motion of the structure in its heave and roll and if elasticity considered, their coupling with the generalised modes of the structure. The vertical displacements along the pontoons are reported over their lengths. The length of Pontoons 1 and 2 are reported with respect to the column supporting Tower 1, and the length of Pontoon 3 is given with respect to the column supporting Tower 2.

Shown in Figs. 8 and 9, the horizontal nodal displacements along the towers and the vertical nodal displacements along the pontoons of the rigid and flexible FOWTs are computed for codirectional waves and wind and compared with those due to combined waves, current and wind at three encounter wave periods, $T_e = 10$ s, 15 s and 24 s.

The structure of the wind-tracing FOWT, due to the asymmetric geometry of the blades and the rotors, is not symmetric with respect to the global x-axis. Therefore, the nodal displacements along Tower 2 are slightly smaller than those of Tower 3 in both rigid and flexible wind-tracing FOWT. The difference between the horizontal nodal displacements along these two towers is attributed to the mode-shape of the complete structure. Commonly, the three flexible towers experience the largest horizontal displacements at encounter wave period $T_e = 24$ s. This is expected, since at approximately $T_e = 24$ s, the surge and pitch RAOs of the flexible wind-tracing FOWT are larger than those of the rigid FOWT.

At $T_e = 10$ s, the towers of the flexible wind-tracing FOWT experience larger nodal displacements compared with the rigid towers in both load conditions. When current is present, shown in Fig. 7, the pitch RAOs of the flexible structure is slightly larger than the rigid structure. As a result, we observe that flexible Tower 2 and 3 undergo larger nodal displacements compared with their rigid-body counterpart. Moreover, the horizontal nodal displacement along Tower 1 is the largest in the absence of current. The different nodal displacements along the towers at a wave period can be attributed to the asymmetry of the wind-tracing FOWT and its mode-shapes.

At $T_e = 15$ s, the presence of current results in small horizontal nodal displacements along flexible Tower 1 in comparison with its rigid counterparts to waves and wind with and without current. Similarly, when current is present, nodal displacements along Tower 2 is the smallest, when the FOWT is flexible. Shown in Fig. 5, it can be seen that when current is added, the surge RAOs of the structure are slightly smaller than its combined waves- and wind-induced surge motion, hence smaller horizontal nodal displacements along the rigid and flexible towers are observed when wave-current interaction is considered. However, at $T_e = 15$ s, it is observed that the current interaction does not influence the nodal displacements along Tower 3 significantly. Furthermore, at $T_e = 24$ s, flexible towers undergo the largest nodal displacements to waves and wind in the absence of current. In conclusion, at the encounter wave periods considered in Fig. 8, the addition of current mostly resulted in smaller horizontal nodal displacements along the three towers.

The vertical nodal displacements along Pontoons 1, 2 and 3 to waves and wind, and combined waves, current and wind are presented in Fig. 9. For the first two encounter wave periods, $T_e = 10$

s and 15 s, smaller differences between the nodal displacements along the rigid and flexible pontoons are observed compared with those at $T_e = 24$ s. Considering encounter wave period $T_e = 10$ s, the vertical nodal displacements along the three rigid pontoons are almost negligible compared with their flexible counterparts. However, it can be seen that the addition of current loads results in larger nodal displacements of flexible Pontoons 1 and 2. As discussed earlier, the structure of the wind-tracing FOWT is not symmetric, and therefore identical vertical displacements along Pontoons 1 and 2 are not observed. At $T_e = 15$ s, it is seen that the largest vertical nodal displacements occur by the flexible pontoons to combined wave, current and wind loads. Similar behaviour is observed at $T_e = 24$ s by flexible Pontoons 2 and 3, which their vertical nodal displacements induced by waves, current and wind are significantly larger than others. Furthermore, $T_e = 24$ s is close to the wet natural period of both flexible and rigid wind-tracing FOWTs in their heave and roll modes. Large vertical displacements along the three pontoons at this encounter wave period, $T_e = 24$ s, could be explained by the resonance behaviour of the structure in its heave and roll natural periods. Nevertheless, it can be seen that the wave-current interaction results in larger hydroelastic motion of the three pontoons at the considered encounter wave periods in Fig. 9.

In this section, the effect of flexibility of the wind turbines and the floating platform of the wind-tracing FOWT on its motion to the environmental loads is discussed. It is shown that surge and pitch RAOs of the flexible FOWT are larger and smaller than their rigid-body counterparts, respectively. Finally, shown in Figs. 8 and 9, the effect of wave-current interaction on the nodal displacements along the towers and the pontoons of the wind-tracing FOWT is presented. It is shown that the presence of current has more significant effect on elastic responses of the pontoons compared with the towers.

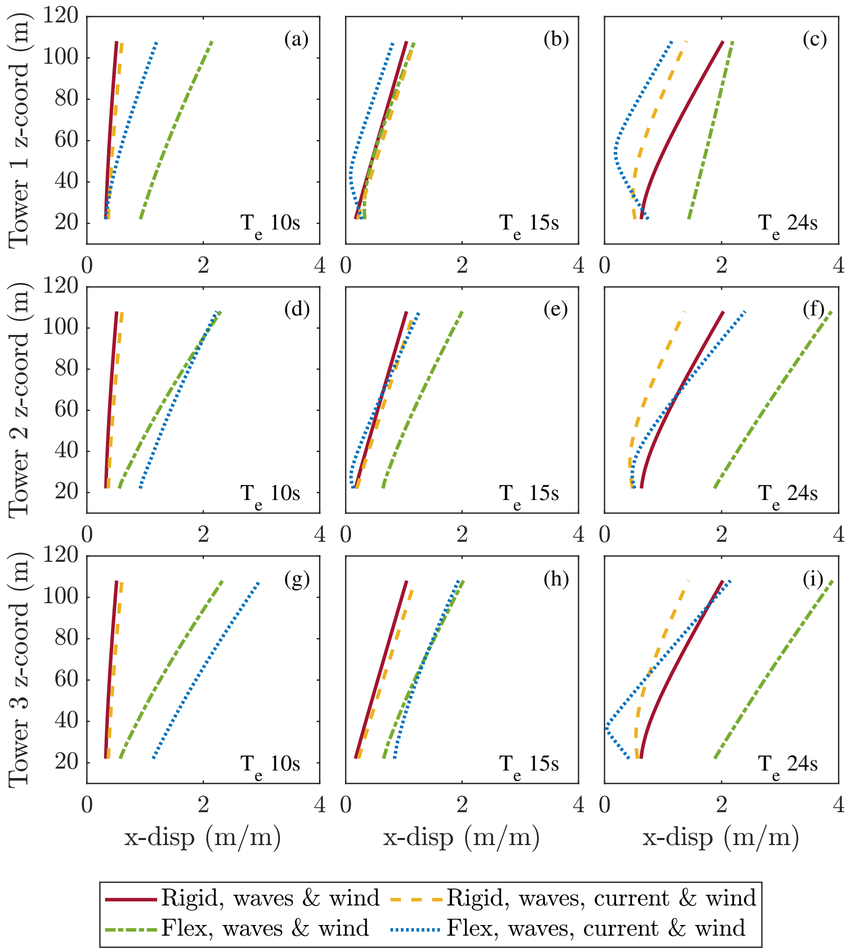

FIG. 8. Horizontal nodal displacements along tower 1 (a), (b) and (c), tower 2 (d), (e) and (f) and tower 3 (g), (h) and (i) at encounter wave periods 10 s, 15 s and 24 s with $V_0 = 11.4$ m/s and $U_c = 0.8$ m/s.

VI. SUMMARY AND CONCLUDING REMARKS

This study investigates the wave-current-wind interaction with the multi-unit wind-tracing FOWT. Dynamic motion of the wind-tracing FOWT to combined wave, current and wind loads is determined by a hydro-aero-elastic numerical coupling approach in the frequency-domain.

In this approach, the governing equations of motions of a floating structure to waves and current in the frequency domain is extended to include the aerodynamic loads on the wind turbines of the FOWT and to obtain elastic motion of the structure, if the elasticity is considered.

The rigid- and flexible-body responses of the wind-tracing FOWT to wave, current and wind are

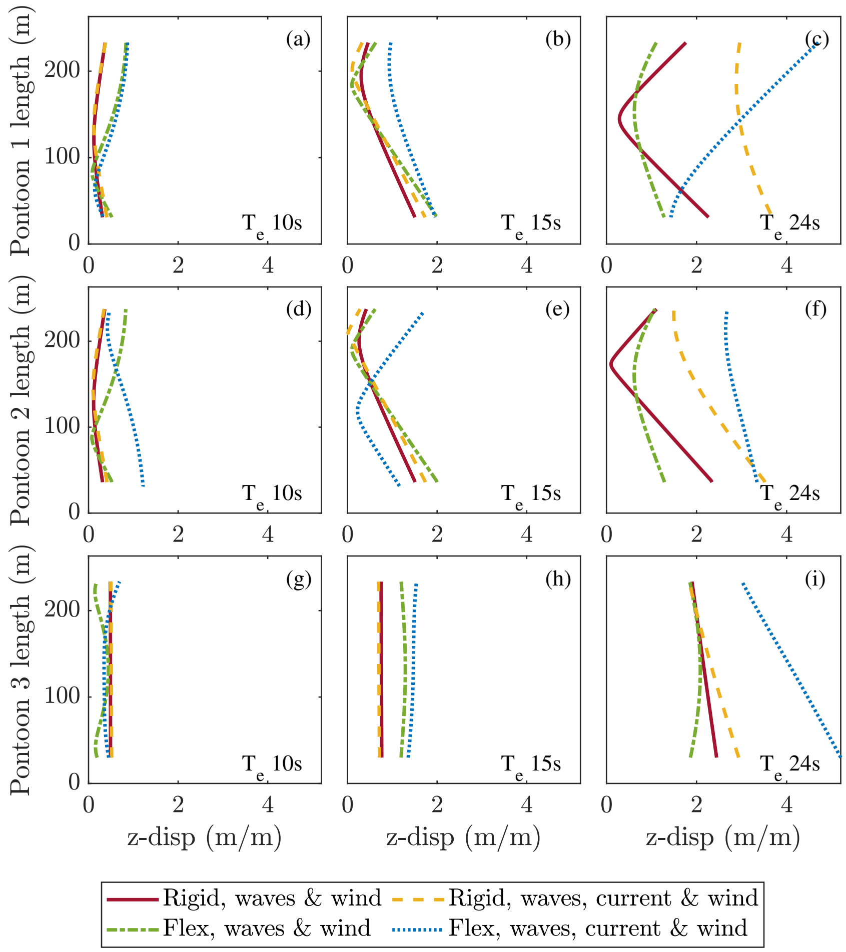

FIG. 9. Vertical nodal displacements along pontoon 1 (a), (b) and (c), pontoon 2 (d), (e) and (f) and pontoon 3 (g), (h) and (i) at encounter wave periods 10 s, 15 s and 24 s with $V_0 = 11.4$ m/s and $U_c = 0.8$ m/s.

calculated and discussed. Firstly, the motion of the rigid FOWT to waves only, combined waves and current and combined waves and wind are compared, and it is seen that its responses are mainly dominated by wave-induced hydrodynamic forces and moments. Next, the rigid-body responses of the FOWT to several current speeds and misalignments between waves with current and wind are presented. It is observed that when aerodynamic loads are present, increasing the current speed results in larger surge and heave motion of the FOWT, whereas the pitch RAOs undergo negligible changes. Furthermore, for encounter wave periods smaller than the pitch natural period of the structures, wave misalignment with current and wind has insignificant effect on the heave and pitch motion of the structure. However, the wind-tracing FOWT undergoes the largest pitch motion when waves, current and wind are codirectional.

Finally, the elastic motion of the wind-tracing FOWT to wave, current and wind loads is obtained and compared with its rigid-body counterpart. Furthermore, the importance of elasticity analysis of the multi-unit wind-tracing FOWT is shown by comparing its rigid- and flexible-body nodal displacements along its towers and pontoons to two environmental conditions, namely *(i)* waves and wind and *(ii)* waves, current and wind. In general, it is observed that the presence of current results in smaller nodal displacements along the towers. However, the wave-current-structure interaction results in larger hydroelastic responses of the wind-tracing FOWT in comparison to those when current is not present and hence larger vertical nodal displacements along the pontoons are obtained.

In conclusion, motion of the wind-tracing FOWT is largely governed by the wave-induced hydrodynamic forces and moments on the substructure and the effect of current with small speed on the hydrodynamic excitation forces and moments on the structure is almost negligible. Consequently, the wind-tracing platform would rotate with respect to the turret such that the moments mainly by the wave-induced hydrodynamic loads on the turret are minimized. This indicates that an appropriate understanding of rigid-body and elastic motion of the substructure plays an important role in analysing the performance of the wind-tracing FOWT. Furthermore, it is also observed that the aerodynamic damping effect by the three operating rotors on the platform influences significantly the surge and pitch motion of the system. Finally, it is seen that when current is present, the hydroelastic responses of the FOWT is affected considerably.

Dynamic analysis of multi-unit FOWTs, due to their unique design and geometrical characteristics, mainly their platform and the mooring layout, are challenging to study. In this paper, it is shown that the developed hydro-aero-elastic coupling approach implemented in HYDRAN-XR can successfully model the environmental loads by waves, current and wind on multi-unit FOWTs and determine their rigid-body and elastic motions. The developed numerical model provides insight about motion of a FOWT concept with an arbitrary shape of the floating platform and number of wind turbines. Therefore, the developed coupling approach can be used in design and concept stages of FOWTs. Nevertheless, it should be noted that a thorough understanding of the effect of nonlinear environmental loads on the performance of the structure, the effect of wind turbine controllers on its power output, and the aerodynamic wake interaction between the wind turbines on a single platform, among others are necessary for design purposes, and should be considered in future studies.

ACKNOWLEDGEMENTS

The work of AL and MH is partially based on funding from the CBJ Ocean Engineering Corp. of Hong Kong. This funding is gratefully acknowledged. Any findings and opinions contained in this paper are those of the authors and do not necessarily reflect the opinions of the funding company.

Conflict of Interest: The authors have no conflicts to disclose.

Data Availability Statement: The data that supports the findings of this study are available within the article.

REFERENCES

Bae, Y. H. and Kim, M., "Coupled dynamic analysis of multiple wind turbines on a large single floater," Ocean Engineering **92**, 175–187 (2014).

Bae, Y. H. and Kim, M. H., "The dynamic coupling effects of a MUFOWT (multiple unit floating offshore wind turbine) with partially broken blade," Journal of Ocean and Wind Energy **2**, 89–97

(2015).

Bashetty, S. and Ozcelik, S., "Design and stability analysis of an offshore floating multi-turbine platform," in *2020 IEEE Green Technologies Conference (GreenTech)* (April 1-3, Oklahoma, United States, 2020) pp. 1–6.

Chen, L., Basu, B., and Nielsen, S. R., "A coupled finite difference mooring dynamics model for floating offshore wind turbine analysis," Ocean Engineering **162**, 304–315, doi:10.1016/j.oceaneng.2018.05.001 (2018).

Chen, X. B. and Malenica, Š., "Interaction Effects of Local Steady Flow on Wave Diffraction-Radiation at Low Forward Speed," International Journal of Offshore and Polar Engineering **8**, 101–109 (1998).

Cheng, P., Huang, Y., and Wan, D., "A numerical model for fully coupled aero-hydrodynamic analysis of floating offshore wind turbine," Ocean Engineering **173**, 183–196 (2019).

Ertekin, R. C., Liu, Y. Z., and Padmanabhan, B., "Interaction of incoming waves with a steady intake-pipe flow," Journal of Offshore Mechanics and Arctic Engineering **116**, 214–220, doi:10.1115/1.2920154 (1994).

Hansen, M. O., Sørensen, J. N., Voutsinas, S., Sørensen, N., and Madsen, H. A., "State of the art in wind turbine aerodynamics and aeroelasticity," Progress in Aerospace Sciences **42**, 285–330 (2006).

Huang, L. L. and Riggs, H. R., "The hydrostatic stiffness of flexible floating structures for linear hydroelasticity," Marine Structures **13**, 91–106 (2000).

Kang, H. Y., Kim, M. H., Kim, K. H., and Hong, K. Y., "Hydroelastic analysis of multi-unit floating offshore wind turbine platform (MUFOWT)," in *Proceedings of the International Offshore and Polar Engineering Conference* (June 25-30, San Francisco, CA, 2017) pp. 554–560.

Kumar, A. and Hayatdavoodi, M., "Effect of currents on nonlinear waves in shallow water," Coastal Engineering **181**, 1–20, doi:10.1016/j.coastaleng.2023.104278 (2023a).

Kumar, A. and Hayatdavoodi, M., "On wave–current interaction in deep and finite water depths," Journal of Ocean Engineering and Marine Energy , 1–21, doi:10.1007/s40722–023–00278–x (2023b).

Lamei, A. and Hayatdavoodi, M., "On motion analysis and elastic response of floating offshore wind turbines," Journal of Ocean Engineering and Marine Energy **6**, 71–90, doi:10.1007/s40722–019–00159–2 (2020).

Lamei, A., Hayatdavoodi, M., and Riggs, H. R., "Hydro- and aero-elastic response of floating offshore wind turbines to combined waves and wind in frequency domain," Journal of Ocean Engineering and Marine Energy , submitted and under review. (2023a).

Lamei, A., Hayatdavoodi, M., and Riggs, H. R., "Motion and elastic response of wind-tracing floating offshore wind turbines," Journal of Ocean Engineering and Marine Energy **9**, 43–67, doi:10.1007/s40722–022–00250–1 (2023b).

Lamei, A., Hayatdavoodi, M., Riggs, H. R., and Ertekin, R. C., "Wave-current-wind interaction with floating offshore wind turbines," Renewable energy , submitted and under review. (2023c).

MacCamy, R. C. and Fuchs, R. A., *Wave forces on piles: A diffraction theory*, Tech. Memo. No. 69 (Beach Erosion Board. Army Corps of Engineers, 1-17, 1954).

Monroy, C., Giorgiutti, Y., and Chen, X.-B., "First and Second Order Wave-Current Interactions for Floating Bodies," in *Volume 1: Offshore Technology*, Vol. 1 (American Society of Mechanical Engineers, 2012) pp. 373–382, doi:10.1115/OMAE2012–83409.

Noblesse, F., Taylor, D., and Chen, X. B., "Decomposition of free-surface effects into wave and near-field components," Ship Technology Research **42**, 167–185 (1995).

Nossen, J., Grue, J., and Palm, E., "Wave forces on three-dimensional floating bodies with small forward speed," Journal of Fluid Mechanics **227**, 135–160, doi:10.1017/S002211209100006X (1991).

NumSoft Technologies,, "HYDRAN-XR, hydrodynamic response analysis with integrated structural finite element analysis, version 23.0," Tech. Rep. (Numsoft Technologies, 2023).

Padmanabhan, B. and Ertekin, R. C., "On the interaction of waves with intake/discharge flows originating from a freely-floating body," Journal of Offshore Mechanics and Arctic Engineering **125**, 41–47, doi:10.1115/1.1537724 (2003).

Padmanabhan, B. and Ertekin, R. C., "Interaction of waves with a steady intake/discharge flow emanating from a 3D body," Journal of Offshore Mechanics and Arctic Engineering **133**, 1–10, doi:10.1115/1.4003057 (2011).

Qu, X., Li, Y., Tang, Y., Hu, Z., Zhang, P., and Yin, T., "Dynamic response of spar-type floating offshore wind turbine in freak wave considering the wave-current interaction effect," Applied Ocean Research **100**, 1–19, doi:10.1016/j.apor.2020.102178 (2020).

Silva, L. S., Cazzolato, B., Sergiienko, N. Y., and Ding, B., "Nonlinear dynamics of a floating offshore wind turbine platform via statistical quadratization — mooring, wave and current interaction," Ocean Engineering **236**, 1–13, doi:10.1016/j.oceaneng.2021.109471 (2021).

Tran, T. T. and Kim, D. H., "Fully coupled aero-hydrodynamic analysis of a semi-submersible fowt using a dynamic fluid body interaction approach," Renewable Energy **92**, 244–261 (2016).

Wong, C., "Wind tracing rotational semi-submerged raft for multi-turbine wind power generation," in *European Wind Energy Association Offshore 2015 Conference* (Copenhagen, Denmark, 2015) pp. 1–10.

Wu, G., "A numerical scheme for calculating the mj terms in wave-current-body interaction problem," Applied Ocean Research **13**, 317–319, doi:10.1016/S0141–1187(05)80055–0 (1991).

Wu, G. X. and Taylor, R. E., "The hydrodynamic force on an oscillating ship with low forward speed," Journal of Fluid Mechanics **211**, 333–353, doi:10.1017/S0022112090001598 (1990).

Wu, Y., *Hydroelasticity of floating bodies*, Ph.D. thesis (1984).

Zhou, Y., Xiao, Q., Liu, Y., Incecik, A., Peyrard, C., Wan, D., Pan, G., and Li, S., "Exploring inflow wind condition on floating offshore wind turbine aerodynamic characterisation and platform motion prediction using blade resolved cfd simulation," Renewable Energy **182**, 1060–1079, doi:10.1016/j.renene.2021.11.010 (2022).